Desalination and Water Treatment
www.deswater.com
doi: 10.5004/dwt.2019.23783

148 (2019) 128–140
April

Oxidative degradation of furfural using synthesized copper activated persulfate in aqueous solution, intermediates identification and artificial neural network modeling

Sahand Jorfi[a], Yaser Tahmasebi Birgani[a], Ali Reza Rahmani[b], Fahime Zamani[b], Mehdi Ahmadi[a], Halime Almasi[a,*]

[a]*Environmental Technologies Research Center, Ahvaz Jundishapur University of Medical Sciences, Ahvaz, Iran, Department of Environmental Health Engineering, Student Research Committee, Ahvaz Jundishapur University of Medical Sciences, Ahvaz, Iran, email: sahand 369@yahoo.com (S. Jorfi), tahmasebiyaser@gmail.com (Y.T. Birgani), ahmadi241@gmail.com (M. Ahmadi), Tel. +989131801815, email: h.almasi14@yahoo.com (H. Almasi)*
[b]*Department of Environmental Health Engineering, Faculty of Health and Research Center for Health Sciences, Hamadan University of Medical Sciences, Hamadan, Iran, email: Rah1340@yahoo.com (A.R. Rahmani), f.zamani2016@yahoo.com (F. Zamani)*

Received 29 July 2018; Accepted 12 January 2019

ABSTRACT

Furfural is an aromatic compound which is mainly used in plastic production and purification of lubricating oils. Furfural removal was investigated using nano-sized zero-valent copper (nZVC or CU•) activated persulfate in aqueous solution by means of artificial neural network modeling. Effect of operational parameters including initial solution pH (3–11), chloride concentration (0.5–4 mM), potassium persulfate (KPS) concentration (0.4–2 mM), Cu nanoparticles dosage (0.01–0.05 g) and furfural concentration (20–100 mg/L) on furfural removal were evaluated. Furthermore, mineralization, kinetic modeling and neural network modeling were also carried out. Result indicated that the highest removal efficiency was achieved at pH 3, nZVC dosage of 0.02 g/L, furfural concentration of 20 mg/L and persulfate concentration of 1.2 mM. In addition, chloride had a dual effect on furfural removal. Neural network modeling also prepared a sensible predictive performance (R^2 = 0.98). By application of artificial neural network (ANN) modeling, a good correlation was obtained with training-validation-data.

Keywords: Artificial neural network; Persulfate; Furfural; Cu nanoparticles; Advanced oxidation technology

1. Introduction

In recent years, lots of synthetic organic chemicals and emerging contaminants have been released into the environment through discharging large amounts of various wastes products in water resources which are the major receiving sinks. Production of these compounds has an increasing trend in the last decades [1–3]. Furfural is a heterocyclic aldehyde ($C_5H_4O_2$), colorless and oily liquid with high solubility in most polar organic solvents. However, it demonstrates moderate solubility of 83 g/L in pure water at 20°C. Furfural and its derivatives such as furfuryl alcohol, alone or with phenol, acetone and urea are used in production of solid resin, plastic and paper. In addition, it is used as a chemical intermediate for the manufacture of furan and tetra furan, which is widely applied in petroleum refineries [4–6]. Consequently, high concentrations of furfural could be found in the effluents of these industries. According to the literature, its concentrations in the effluent rubber and plastic products manufacturing, furfural production and oil refining have been reported to be 1700, 600 and 500 mg/L, respectively [7]. Acute exposures to furfural can potentially lead to lung, liver and kidney damage and the long-term exposure effects are tumor growth and mutagenesis [7]. Several methods such as physical, chemical and biological approaches of furfural

*Corresponding author.

removal from aqueous solution have been used so far [4,8]. Adsorption is proved as an effective and promising technology for removal of pollutants from aqueous solution. However, the cost of adsorbent production is expensive which made researchers to investigate the alternative methods for removal of pollutants [9]. Biological treatment processes are time-consuming, work-demanding, and inefficient in the case of persistent organic molecules and are sensitive to environmental conditions [10]. Advanced oxidation processes (AOP) have been welcomed by different researchers, because of their high efficiency, short required reaction time and wide range of applications. Recently, production of sulfate radicals has been known as a promising AOP for removal of organic pollutants. Persulfate (PS) is a powerful oxidizing agent with the oxidation reduction potential (ORP) of 2.0 V. It can be activated by heat, light or metal ions and converted to sulfate radical with ORP of 2.6 V [11]. Additionally, sulfate radical with longer half-life has higher ability than hydroxyl radical for oxidizing organic molecules [9]. PS -as a source of sulfate radical- has demonstrated the large stability at room temperature and aqueous media. Thermal and chemical (transition metal) processes are the most applied common activation methods for PS as Eqs. (1) and (2) [9].

$$S_2O_8^{2-} + heat\ /\ UV \rightarrow 2SO_4^{\bullet-} \quad (1)$$

$$S_2O_8^{2-} + (Me^{n+}) \rightarrow SO_4^{\bullet-} + (Me^{n+1}) + SO_4^{2-} \quad (2)$$

Other studies have reported that the sulfate and hydroxide radicals are formed when PS is activated, according to Eqs. (3) and (4) [12,13]

$$\text{All pH} = {}^{\bullet}SO_4^{-} + H_2O_2 \rightarrow SO_4^{2-} + {}^{\bullet}OH + H^+ \quad (3)$$

$$\text{Alkaline pH} = {}^{\bullet}SO_4^{-} + OH^- \rightarrow SO_4^{2-} + {}^{\bullet}OH \quad (4)$$

This distribution is strongly pH-dependent. Sulfate radical dominates at pH values of less than 7, while hydroxyl radical was dominated at pH values higher than 9 and both sulfate radicals and hydroxyl radicals were dominated at pH 7–9, and superoxide anion can be generated under alkaline pH, as shown in Eqs. (5)–(7) [12,14–16].

$$S_2O_8^{2-} + H_2O \rightarrow SO_4^{2-}2H^+ \quad (5)$$

$$SO_5^{2-} + H_2O \rightarrow HOO^- + SO_4^{2-} + H^+ \quad (6)$$

$$HOO^- + S_2O_8^{2-} \rightarrow {}^{\bullet}SO_4^{-} + SO_4^{2-} + H^+ + {}^{\bullet}O_2^{-} \quad (7)$$

In addition, sulfate radical is more selective oxidant than hydroxyl radical to remove persistent organic pollutants [17]. Copper oxide has been widely applied for activation of PS, due to low energy input, low or no need for pH adjustment and acceptable oxidative performance in neutral conditions [18]. In previous studies, many transition ions have been used to activate PS, but all the transition ions are not efficient. Copper is a high redox transition metal remain usually in the oxidation states of Cu(I) and Cu(II) [18,19]. Recently, considerable attentions have been paid to copper nanoparticles as adsorbents or catalysts, due to high specific surface area, insolubility in water, catalytic reactivity and high adsorption capacity [20,21]. Zerovalent copper exhibited a faster removal rate of organic compounds compared to zerovalent iron, due to the high reactivity. Another aim of the present study was investigation of a suitable artificial neural network (ANN) model for predicting furfural removal from aqueous solution. ANN is a nonlinear mathematical model which describes the inputs and outputs parameters of a typical system [22]. Two favorite ANNs are (i) multiplayer feed-forward neural network trained by back propagation algorithm which is widely used in research, and (ii) Kohonen self-organizing mapping [23]. The application of ANN analysis to solve the environmental engineering problems has been the topic of different review studies [23] such as biological treatment [24] and reductive removal [25]. Commonly used ANNs include multilayer perception (MLP), self-organization mapping (SOM), radial basis function (RBF) and fuzzy network [26,27]. Regarding the advantages of advanced oxidation processes for removal of organic compounds, in particular furfural, interest on PS activation with copper, the main aim of current work was investigation of the effect of PS/ZVC for furfural removal. Moreover, the influence of input variables on the process efficiency was examined.

2. Experimental

2.1. Chemical and apparatus

All chemicals such as $CuSO_4$, sodium borohydride, ethanol, sodium hydroxide, sulfuric acid, potassium PS and furfural were of analytical grade and prepared from Merck, Germany. pH of solution was measured via a pH-meter (pH.Z.S.PTR79, Germany). A UV–vis spectrophotometer (DR6000, Hach USA) was utilized to determine the furfural concentrations. The surface characteristics and elemental analysis of Cu nanoparticles were carried out using field-emission scanning electron microscopy by means of a TESCAN microscope (FE-SEM, Mira 3, Czech Republic) equipped with energy dispersive X-ray (EDX) microanalysis. The X-ray diffraction (XRD) patterns of Cu nanoparticles were recorded by an X-ray diffractometer (Model: GNR-MPD3000) using Cu anode at λ = 0.15060 nm, voltage at 40 kV, and current intensity = 30 mA. Fourier transforms infrared (FTIR NICOLET 380) spectroscopy analyses were used to explain the presence of functional groups on the surfaces of Cu nanoparticles. Total organic carbon (TOC) was determined via a TOC analyzer (Shimadzu, TOC-VCSH, Japan) for exploring the mineralization of furfural.

2.2. Synthesis of ZVC Nanoparticles

In this study, nZVC was synthesized by chemical reduction approach [28]. In this regards, a specific quantity of copper sulfate was added to deionized water to obtain blue solution. In order to remove oxygen from solution, nitrogen gas was purged for about 10 min. The borohydride solution (0.37/10 mL) was gently added into the solution while fast stirring. In this step, light blue color solution was changed from orange to dark red and black [29]. The reaction has to be carried out under a hood, due to the production of hydro-

gen gas as a by-product. After the reaction, the nanoparticles were deposited as a black precipitate. The appearance of the dark color showed that the reduction reaction was started. To complete experiments, the reaction solution exposed to ambient atmosphere for another 10 min [29].

2.3. Experimental procedure

All experiments were carried out in batch mode in a 250 mL glass beaker. Effect of operational parameters including solution pH (3–11), chloride anion concentration (0.5–4 mM), potassium persulfate (KPS) concentration (0.4–2 mM), Cu nanoparticles (0.01–0.05 g/L) and furfural concentrations (20–100 mg/L) were studied consecutively, according to one factor at the time methodology. Adjusting of the solution pH was performed using sulfuric acid (1 N) and NaOH (1 N) solutions. Sampling was performed at regular time intervals, centrifuged (6000 rpm for 2 min) and then the residual furfural concentration was measured using a UV-visible spectrophotometer (model: HACH LPV441.99.00002_28) at the wavelength of 277 nm. The furfural removal efficiency (%) was obtained according to Eq. (8):

$$\text{Removal (\%)} = C_0 - C_t/C_0 \times 100 \quad (8)$$

where C_0 and C_t are initial and residual furfural concentrations (mg/L) at specified reaction time t (min), respectively.

2.4. Artificial neural networks (ANNs) modeling

ANN - as a nonlinear mathematical model - can solve complex nonlinear processes which are not appropriate for common methods. Multi-layer perceptron (MLP) is a supervised learning algorithm with either one or more hidden layers. In this work, applied MLP has a three layers containing input, a hidden and output layers. A training algorithm was used as an optimization of neural network modeling. Implementing the suitable functions, weights and bias are essential for application of MLP model [22]. To compare the predicted outputs with experimental ones, weight and bias values were adjusted progressively during the training phase. These networks are trained using the back propagation algorithm. In this work, ANN was used by the Levenberg–Marquardt method. The most transfer functions which are applied for developing MLP are indicated as follows [22]:

$$\text{Sigmoidal : } F(x) = \frac{1}{(1+\exp(-X))}$$

$$\text{Tansig: } F(x) = \frac{2}{(1+\exp(-2X))}$$

In this study, the attributed data were included 5 inputs (pH-Cu-furfural-PS-Time) and one output (the percentage of furfural removal). The applied ANN was back propagation (Fig. 1). This algorithm has many training and ability to rapidly attain convergence in the training process [30]. The training system is performed by means of making changes to the weights, due to approach the desired output to target. Fig. 1 indicates the architecture of artificial neural network back propagation with hidden layers.

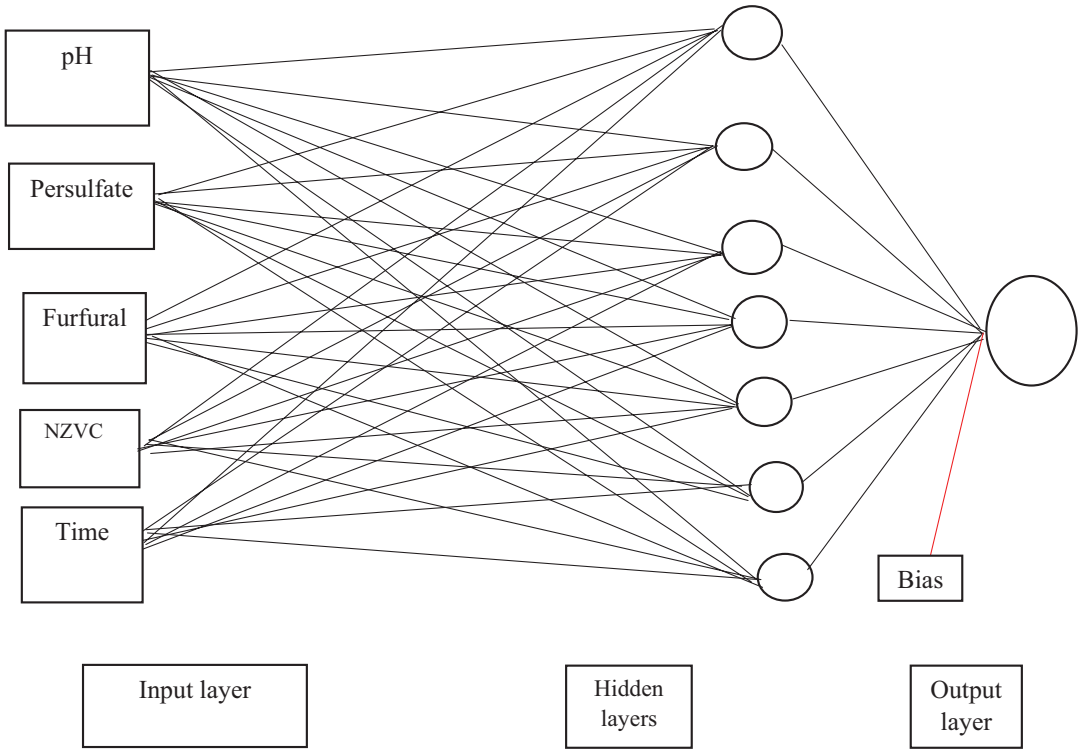

Fig. 1. Neural network architecture system.

3. Results and discussion

3.1. Characterization of nZVC

The particle size and evolution of surface morphology of nZVC were analyzed using field emission scanning electron microscopy (FE-SEM), together with EDX analysis (Figs. 2a and b). Copper nanoparticles had a mono-dispersed distribution of average particle. The sizes are found in the range of 15–23 nm [31]. According to Fig. 3, there are three diffraction sharp peaks at around 2θ = 42.51, 50.56 and 74.20 which correspond to 1800, 4000, 1700 and 1000, respectively due to nano-crystalline properties of Cu• [31,32]. Also, two small peaks exist at 36.61 and 61.64° which show that a portion of copper is degraded and changed into Cu_2O, confirming face centered cubic (FCC) crystal formation [32]. The average crystalline size of Cu nanoparticles was calculated using Scherer's equation [Eq. (9)] and found to be 15.36–23.28 nm [32]. The average crystalline size of Cu nanoparticles was in good agreement with those observed in FE-SEM images.

$$D = 0.9\lambda / \beta\cos\theta \quad (9)$$

where, D is the diameter of nanoparticles, λ is the X-ray wavelength and β is the full-width at half-maximum.

Fourier transform infrared spectroscopy (FTIR) detects the absorption of radiation and the mutations and molecular vibrations couple of atomic ions [33]. This method is mainly used to identify organic compounds, because the spectra of these compounds are usually complex and have a large number of maximum and minimum peaks that can be used for comparative purposes. FTIR spectra provided information about the nature of copper nanoparticle which are necessary to confirm the purity of copper [33]. Fig. 4 indicates the FTIR spectra of copper nanoparticles including bands at 635, 1069–1130, 1333–1402, 1635, 3437 cm^{-1}. These bands belong to Cu_2O, NO_3, C=O bond, H-O-H bending and O–H stretching, respectively. This work agreed with Kayani et al. and Suresh et al. [32,33].

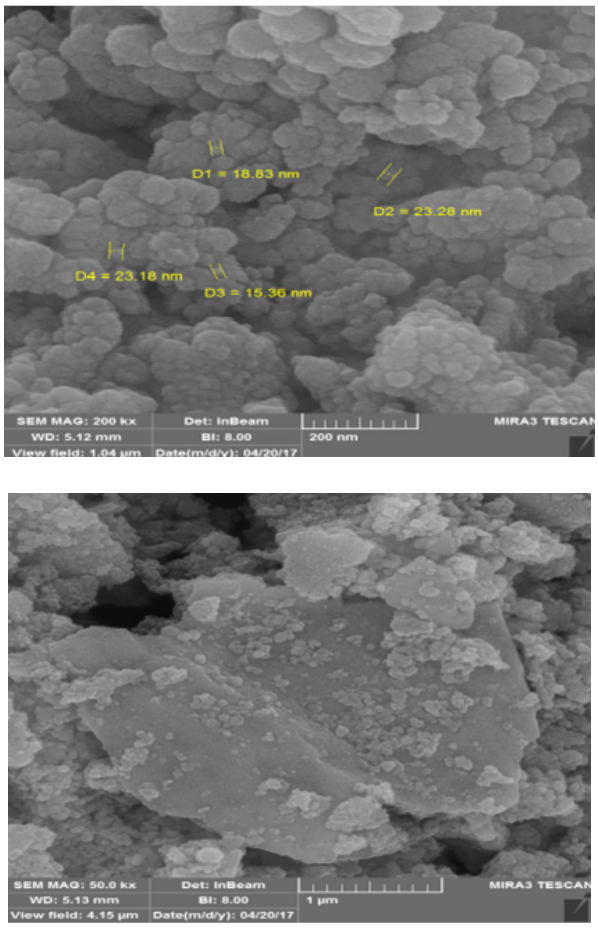

Fig. 2a. SEM pattern of copper nanoparticles.

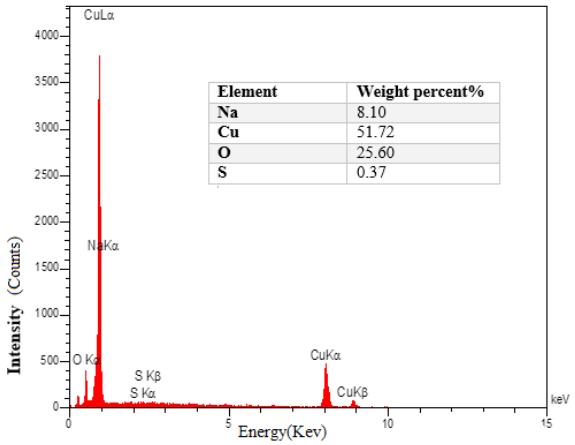

Fig. 2b. EDX pattern of copper nanoparticles.

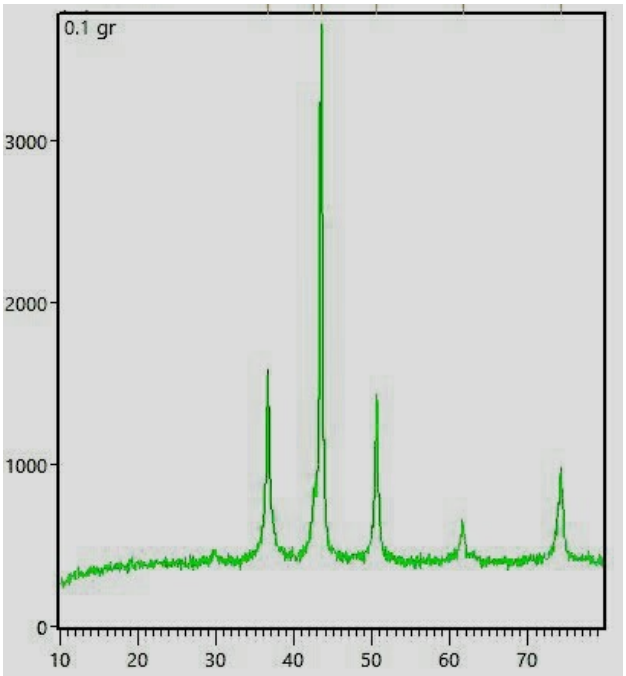

Fig. 3. XRD pattern of copper nanoparticles.

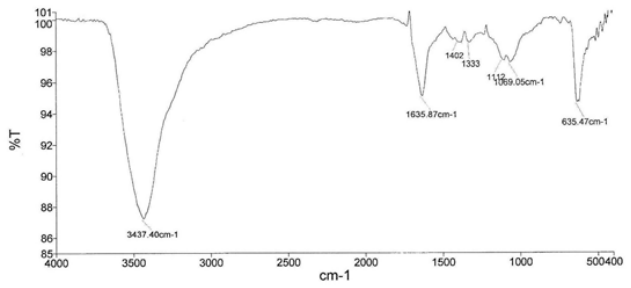

Fig. 4. FTIR pattern of copper nanoparticles.

3.2. Cu nanoparticles activated PS process

3.2.1. Effect of initial pH

The solution pH generally has a significant role in degradation of organic contaminants [34]. The influence of solution pH (3–11) on PS/CU• process was studied (Fig. 5a) at furfural concentration of 20 mg/L, PS concentration of 0.8 mM and Cu• concentration of 0.02 g/L. Results indicated that furfural was rapidly degraded at pH = 3 and the lower pH values favored furfural degradation. Removal efficiencies of 59.24, 44.21, 30.14 and 15.61% were observed at pH 5, 7, 9 and 11, respectively. Similar results were reported by Peng et al. [19]. At pH 4 or higher, the absence of H^+ prevented the Cu^+ release and greatly reduced the removal efficiency. While, the presence of PS considerably enhanced the degradation of ZVC and Cu^+ release, particularly in pH of < 4. This result agreed with Zhou et al. [35]. On the other hand, a decrease in removal was observed along with an increase in pH in the range of neutral and alkaline conditions. This result agreed with Wang et al. [36]. Chemical reaction of PS is strongly pH-dependent. In acidic conditions, furfural decomposition rate is facilitated and solution pH is an important factor for the activation of PS by nZVC [19]. When pH is over 5, the strong hydrolysis of copper in neutral and alkaline conditions may prevent activation of PS [36]. In addition, it was supposed that H^+ could simplify the decomposition of furfural with dissolving nZVC in acidic conditions [19]. Furthermore, OH^- prevents the Cu^+ in decomposition of CuOH to Cu_2O and H_2O via Eqs. (10) and (11).

$$Cu^{2+} + OH^- \rightarrow CuOH \tag{10}$$

$$2CuOH \rightarrow Cu_2O + H_2O \tag{11}$$

3.2.2. Effect of PS concentration

PS, as a source of active species, is the main factor in the ZVC/PS process [37]. Results showed that the degradation of furfural increased with increasing PS concentration. The highest removal efficiency was observed at pH 3 and PS concentration 1.2 mM. According to Fig. 5b, when PS concentration was increased from 0.4 to 1.2 mM, the furfural degradation increased from 53.45 to 97.96%, due to the production of more sulfate radicals [38]. But, in comparison with furfural decomposition, when PS concentration was increased to above 1.2 mM, removal efficiency was decreased. Similar findings have been reported by Wang et al. [37]. When PS cocentration increased over an optimum level, sulfate radicals react with excess PS concentrations and produce $^{\bullet}SO_4^{2-}$ that is a scavenger of sulfate radicals and the removal efficiency was decreased according to Eq. (12).

$$S_2O_8^{2-} + {}^{\bullet}SO_4^- \rightarrow S_2O_8^- + SO_4^{2-} \tag{12}$$

3.2.3. Effect of nZVC dosage

Fig. 5c indicates the effect of different nZVC dosages (0.01–0.05 g) on removal of furfural under the following experimental conditions: pH = 3, PS concentration: 1.2 mM and furfural concentration: 20 mg/L. The addition of nZVC enhanced the removal efficiencies of furfural to 58.28, 97.96, 80.38, 85.63 and 79.3 % for nZVC dosages of 0.1, 0.2, 0.3, 0.4 and 0.5 g/L, respectively. nZVC as a source of copper ion was applied for activation of PS, based on the following equations: [13–15]: [38].

$$2Cu + HSO_5^- + H^+ \rightarrow 2Cu^+ + SO_4^{2-} + H_2O \tag{13}$$

$$2Cu + HSO_5^- \rightarrow Cu^+ + {}^{\bullet}SO_5^- + OH^- \tag{14}$$

$$Cu^{2+} + HSO_5^- \rightarrow Cu^+ + {}^{\bullet}SO_5^- + H^+ \tag{15}$$

According to Fig. 5C, with increasing nZVC dosage, the removal efficiency increased significantly. The results are in agreement with Ghanbari et al. [38]. An improvement in furfural degradation rate via increasing nZVC dosage is due to the enhancement of Cu^+ generation resulting in production of a large amount of reactive radicals [19]. But, further enhancement in nZVC dosage over 0.2 g/L resulted in decreasing furfural removal [39,40]. Results indicated that at higher ZVC dosages, nZVC/PS process released more Cu^+, much of it would be quenched by reactive radicals [Eqs. (16) and (17)] [35] and the removal efficiency has been decreased [Eqs. (16) and (17)].

$$Cu^+ + SO_4^- \rightarrow Cu^{2+} + {}^{\bullet}SO_4^{2-} \tag{16}$$

$$Cu^+ + OH^{\bullet} \rightarrow Cu^{2+} + OH^- \tag{17}$$

3.2.4. Effect of furfural concentration

According to Fig. 5d, when furfural concentration increased to 10, 20, 40, 60 and 80 mg/L, the removal rates decreased from 100 to 97.96, 79.78, 55.15 and 39.32% after 60 min, respectively. Obviously, increasing the initial pollutant concentration would decrease the possibility of reaction between the molecules and those of reactant species. The intermediate compounds generated during the reaction can develop by products and consume hydroxyl radicals and sulfate. This evidence can potentially cause a competition between main pollutants and intermediate metabolites while reacting with radicals [41,42].

3.2.5. Effect of chloride anion

To identify the effect of scavenging ions, several experiments were carried out in the presence of chloride

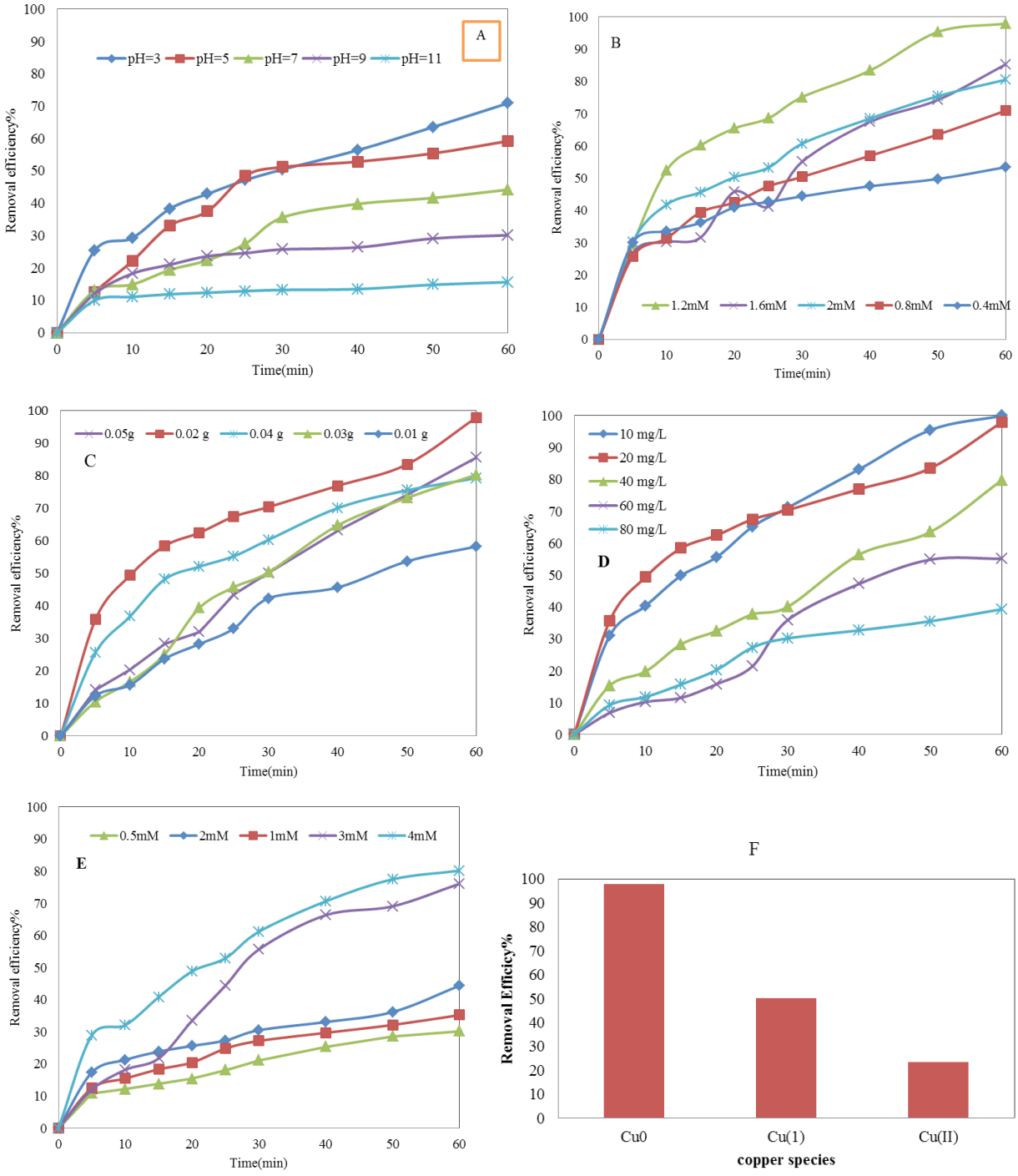

Fig. 5. Effect of operational parameters on furfural removal using Cu nanoparticles activated persulfate process (A) Effect of initial pH (furfural: 20 mg/L, PS: 0.8 mM and nZVC = 0.02 g/L) (B) Effect of persulfate concentration (furfural: 20 mg/L, pH = 3 and nZVC = 0.02 g/L), (C) Effect of nZVC dosage (furfural: 20 mg/L, pH = 3 and PS = 1.2 mM/L), (D) Effect of furfural concentration (PS: 1.2 mM, pH = 3 and nZVC = 0.02 g/L), (E) Effect of chloride ion (furfural: 20 mg/L, pH = 3, PS: 1.2 mM and nZVC = 0.02 g/L), (F) Effect of copper species (furfural: 20 mg/L, pH = 3, PS: 1.2 mM and nZVC = 0.02 g).

ions (Cl^-). Cl^- is one of the scavenging ions affecting the accessibility of $^{\bullet}SO_4^-$ in process [43]. According to Fig. 5E, addition of Cl^- (0.5 and 1 M) significantly prevented furfural degradation in all investigated runs. Preventing the degradation of furfural can be explained by impeding $^{\bullet}SO_4^{2-}$ production through addition of choloride ions. Actually, Cl^- ions react with $^{\bullet}SO_4^-$ to produce $Cl^{\bullet}$ and free chlorine [Eq. (18)] which quickly mix with the other chloride ions and form dechloride radical anion ($Cl_2^{\bullet -}$)[Eqs. (18)–(21)] [44].

$$^{\bullet}SO_4^- + Cl^- \rightarrow Cl^{\bullet} + {}^{\bullet}SO_4^{2-} \quad K_{^{\bullet}SO_4^-,Cl^-} = 2.0\times10^8 M^{1-}S^- \quad E^0 = Cl^{\bullet}/Cl^- = 2.41V \quad (18)$$

$$Cl^{\bullet} + Cl^- \rightarrow Cl^{\bullet} + {}^{\bullet}SO_4^{2-} \quad K_{^{\bullet}Cl^-,Cl^-} = 0.8 - 2.1\times10^{10} M^{1-}S^- \quad E^0 = Cl^{\bullet}/Cl^- = 2.09C \quad (19)$$

$$^{\bullet}Cl_2^- + {}^{\bullet}Cl_2^- \rightarrow 2Cl^- + Cl_2^- \quad K = 1.3\times10^9 M^{1-}S^- \quad E^0 = Cl^{\bullet}/Cl^- = 1.36V \quad (20)$$

$$Cl_{2(aq)} + H_2O \rightarrow HOCl + H^+ + Cl^- \qquad E^0 = HOCl/Cl^- = 1.48V \quad (21)$$

As can be seen from Fig. 5E, the existence of low concentrations of Cl^- (1–2 mM) prevented furfural removal, while high concentrations of Cl^- (3–4 mM) caused increasing degradation rate [45]. Results of this study are in line with the dual effects of Cl^- reported in the other studies [46]. Cl^-, at low concentrations can react with sulfate radical, due to the remarkable reaction rate constant. But, only small amount of the corresponding Cl^- can react with radicals and free chlorine species might be generated at low Cl^- concentrations [43]. Thus, Cl^- played an important role as $^{\bullet}SO_4^-$ scavenger, which led to gradual degradation of furfural. The removal efficiency showed a slight increase with further increase in the reactive chlorinated radicals and free chlorine Cl^- concentration [43]. The oxidation-reduction potential of Cl^- radicals is less than sulfate radical and the chlorine species belong to moderate oxidationts, which participate in furfural oxidation. Wang et al. displayed that $^{\bullet}SO_4^-$ and PS can participate in reactions with Cl^- that is in accordance with the findings of this study [43].

3.2.6. Effect of copper species on PS activation

Effect of copper species including Cu^+, Cu^{2+} and nZVC on furfural removal rate were investigated under optimun levels (pH = 3, furfural concentration of 20 mg/L and PS of 1.2 mM). According to Fig. 5f, the obtained removal rates for Cu^+, Cu^{2+} and nZVC were 23.5, 63.21 and 97.96 %, respectively. For nZVC, Cu^+ has an important influence on activating PS, which is immediately converted to Cu^{2+} by either oxygen or the other oxidants in the solution [Eqs. (22)–(24)] [35]. This result agreed with Raut et al. [40].

$$2\,Cu^{\bullet} + 2H^+ \rightarrow 2\,Cu^{\bullet} + H_2 \quad (22)$$

$$2\,Cu^{\bullet} + S_2O_8^{2-} \rightarrow 2\,Cu^+ + 2\,SO_4^{2-} \quad (23)$$

$$2\,Cu^{\bullet} + HSO_5^- \rightarrow 2\,Cu^+ + SO_4^{2-} + H^+ \quad (24)$$

Wen et al. reported that Cu^+ is a critical factor in degradation of nZVC and production of hydroxyl radicals in acidic conditions [47]. It can be proved that Cu^+ is the most reactive copper species that generates hydroxyl and sulfate in the PS/nZVC process, according to Eqs. (25)–(27). In addition, nZVC produces reactive radicals through direct activation of PS, but acts as a barrier against furfural degradation by chelating copper. The direct activation of PS by nZVC takes place slightly [47]. This result agreed with Peng et al. [19].

$$HSO_5^- + M^{n+} \rightarrow M^{(n+1)+} + {}^{\bullet}SO_4^- + OH^- \quad (25)$$

$$HSO_5^- + M^{n+} \rightarrow M^{(n+1)+} + SO_4^{2-} + OH^{\bullet} \quad (26)$$

$$HSO_5^- + M^{(n+1)+} \rightarrow M^{n+} + SO^{\bullet}{}_5^- + H^+ \quad (27)$$

3.2.7. Reaction mechanism

As mentioned above, the reactions of PS were probably activated by copper and sulfate free radicals in acidic conditions, especially in pH 3, considering that a high level of copper ions according to Eq. (28), and $^{\bullet}SO_4^-$ were formed [39]. While, when pH increased to 5, a decrease was happened in H^+ and copper ions and then PS immediately reacted with copper to produce free sulfate radical, as shown in Eq. (29).

$$CuO + 2H^+ \rightarrow Cu^{2+} + H_2O \quad (28)$$

$$CuO + S_2O_8^{2-} + 2H^+ \rightarrow Cu^{3+} + {}^{\bullet}SO_4^{2-} + H_2O \quad (29)$$

With increasing pH to 7, copper ion concentration became less than previous stage and the dominant reaction of sulfate free radicals comes into Eq. (19). In alkaline conditions (pH = 11), the sulfate free radical prevailing by basis-activated and hydroxyl radicals was pravalent, based on Eqs. (30), (31).

$$S_2O_8^{2-} + 2H_2O \rightarrow {}^{\bullet}SO_4^- + 3SO_4^{2-} + {}^{\bullet}O_2^- + 4H^+ \quad (30)$$

$$^{\bullet}SO_4^- + OH^- \rightarrow SO_4^{2-} + OH \quad (31)$$

It has been reported that $^{\bullet}SO_4^-$ is a dominant radical in acidic conditions. But, $OH^{\bullet}$ is the most dominant radical at alkaline pH values [39,47]. In addition, the presence of sulfate free radical can affect exchange reaction to generate hydroxyl ions which have a higher oxidation potential than sulfate free radical ($^{\bullet}SO_4^-$) as Eq. (3). However, both sulfate and hydroxide radicals are responsible for degradation of contaminant in PS/nZVC process. In order to understand which type of radical involves in the degradation process and the effect of radical scavengers, methyl alcoholor (MA) and tert butyl alcohol (TBA) were used [39,48]. It is observed that $SO_4^{\bullet}$, $SO_5^{\bullet}$, and $\cdot OH$ could be generated for activation of PS by transition metals. Each of the three radicals are formed during PS/nZVC system. During the reaction, nZVC has an important pattern in PS inactivation, thereby production of activated radicals [39,49]. $MA(K = 8\times10^5 M^{-1}S^{-1})$ is one of the most comon quenchers for both $^{\bullet}SO_4^-$ and $^{\bullet}OH$ [47]. TBA is another quencher for $^{\bullet}OH$ but not applicable for $^{\bullet}SO_4^-$. Concurrently, $SO_5^{\bullet-}$ is relatively quiescent to MA and TBA with low rate. As a result, the total removal of furfural was obtained in 60 min in PS/nZVC process, but, decreased to 4.5 % via addition of 3 mM MA, which rejected the share of $SO_5^{\bullet-}$ on furfural degradation. Also, 51.35 % of furfural was decomposed in PS/nZVC process via addition of 3 mM TBA. Therefore, it can be concluded that $^{\bullet}OH$ and $SO_4^{\bullet-}$ were the main reactive radicals in PS/nZVC process. This parameter agreed with Peng et al. [19].

3.2.8. Mineralization

Intermediate compund can be generated by oxidation of furfural. Chemical oxygen demand (COD) and total

organic carbon (TOC) concentrations were determined as index of organics in reaction solution [38]. Fig. 6 shows the removal of organic material by measurement of COD and TOC at 60 min. COD and TOC removal rates were 75.56 and 31.10%, respectively. Generally, COD [50] removal was significantly higher than the TOC removal which can be due to the oxidation molecules containing of furfural to stable organic materials which cannot reduce TOC value. This study agreed with Kang et al. [51]. The average oxidation state (AOS) is a concept which shows the mineralization rate of organic pollutant [Eq. (32)] [38,52].

$$AOS = \frac{(TOC - COD)}{TOC} \quad (32)$$

The range of AOS can be varied between + 4 and –4. AOS = 4 is means of the most oxidized form of carbon and it is belong to the carbon dioxide. AOS = –4 is ascribe to the methan which is the most reduced form of carbon [52]. Result showed AOS values for furfural after and before treatment are 2 and –0.32 respectively. Results showed that furfural is not easily mineralized to CO_2 and H_2O and the organic intermediate compounds were formed during the reaction.

3.2.9. Intermidates of furfural degradation

Figs. 7a and b show the GC-MS analysis of furfural degradation (1 and 24 h). Generally, the organic pollutants are not degraded to CO_2 and H_2O completely, but organic intermediates are produced in many cases [38]. Results indicated that the main intermediates of furfural degradation were ferulic acid, 2-furfural, oxime-, methoxy-phenyl, and 2,2′-bifuran. Two dominant peaks related to 2-furaldehyde and 2,2′-bifuran were observed at reaction time of 24 h. Results revealed that with increasing the reaction time, hazardous compounds were oxidized and converted into harmless compounds, which is in agreement with findings of Li et al. [51].

3.2.10. Catalyst reusability

To recognize the reusability potential of nZVC, the experiments were carried out in four continuous steps at the following operational conditions: initial furfural concentration = 20 mg/L, nZVC dosage = 0.02 g, initial pH = 3, PS = 1.2 mM and and reaction time = 60 min. After each step, the consumed zNVC was chemically regenerated by 0.1 M H_2SO_4 at 30 min. The removal efficiencies of furfural (%) at the first, second, third and fourth steps were 97, 60.87, 53.54 and 49.71%, respectively. The obtained findings revealed that the loss in the furfural removal after three consecutive cycles was nearly 21%, confirming that nZVC can be applied as a stable material via high recovery potential [53]. The reduction of furfural removal may be attributed to the protonation of nZVC surfaces after chemical recovery that caused positive charged surfaces of nZVC [53]. Moreover, the recycling runs may lead to the loss of nZVC thereby sedimentation of the nano particle surface by the intermediates of PS and nZVC. The results of atomic absorption spectrometry indicated that a negligible amount of nZVC was released into the solution during the reactions of furfural removal (0.2 mg/L), which can be assumed non-hazardous, consistent with the limited amount of 1 mg/L [54]. This result was authenticated by findings of SEM and EDX analyses.

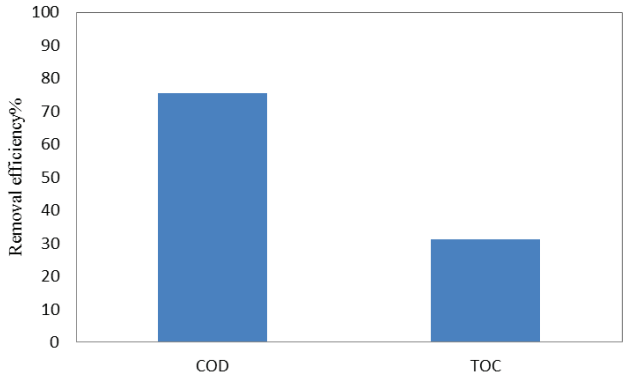

Fig. 6. COD & TOC removal in selected conditions (furfural: 20 mg/L, PS: 1.2 mM, pH = 3, mM and nZVC = 0.02 g).

3.2.11. Kinetic study

Fig. 8 indicates the kinetic studies of furfural degradation in nZVC/PS process. Chemical kinetics were applied

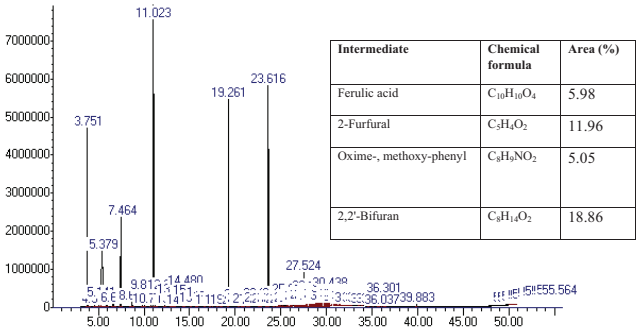

Intermediate	Chemical formula	Area (%)
Ferulic acid	$C_{10}H_{10}O_4$	5.98
2-Furfural	$C_5H_4O_2$	11.96
Oxime-, methoxy-phenyl	$C_8H_9NO_2$	5.05
2,2'-Bifuran	$C_8H_{14}O_2$	18.86

(A)

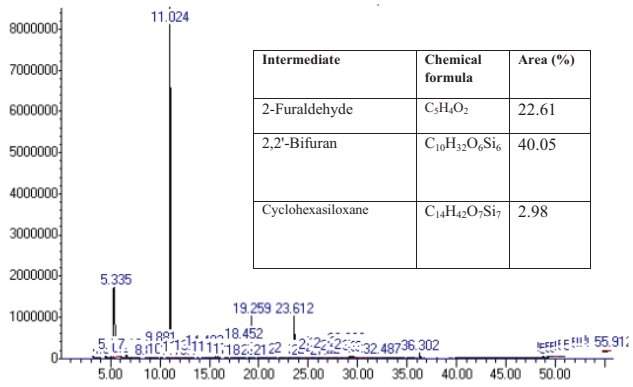

Intermediate	Chemical formula	Area (%)
2-Furaldehyde	$C_5H_4O_2$	22.61
2,2'-Bifuran	$C_{10}H_{32}O_6Si_6$	40.05
Cyclohexasiloxane	$C_{14}H_{42}O_7Si_7$	2.98

(B)

Fig. 7. GC-MS chromatogram of intermediates of furfural degradation after (A) 1 h, (furfural: 20 mg/L, PS: 1.2 mM, pH = 3, mM and nZVC = 0.02 g), (B) 24 h, (furfural: 20 mg/L, PS: 1.2 mM, pH = 3, mM and nZVC = 0.02 g).

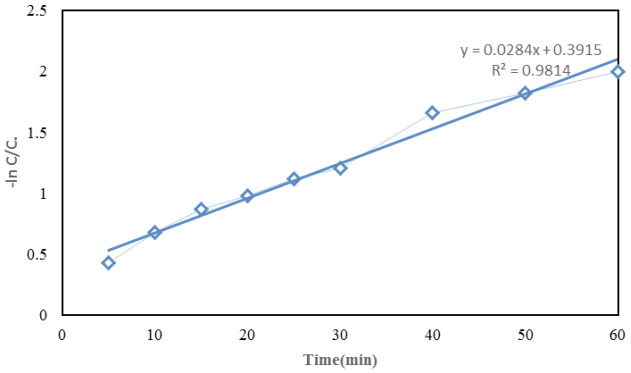

Fig. 8. Kinetic studies of furfural degradation (furfural: 20 mg/L, PS: 1.2 mM, pH = 3, mM and nZVC = 0.02 g).

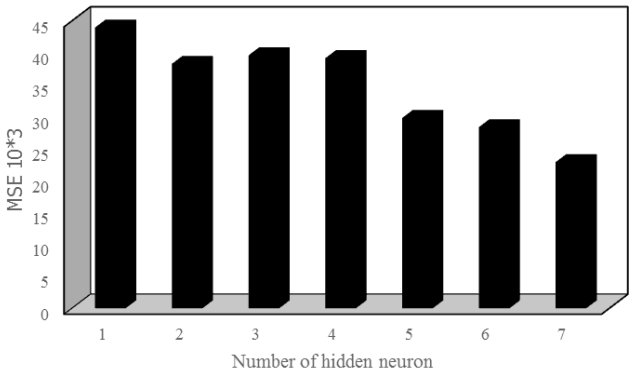

Fig. 9. Effect of the number of neurons in the hidden layer on the performance of neural network.

to study the chemical reaction rate. Based on the obtained results of reaction kinetics under optimum conditions (initial furfural concentration: 20 mg/L, PS: 1.2 mM, pH = 3 and nZVC dosage = 0.02 g), the furfural removal follows first-order kinetics model. For zero-order kinetics model, the half-life is independent of the initial concentrations of reactants, while for first and second-order reactions, half-life was different with initial concentrations [55]. The nZVC/PS consumption data were proportionate to a first-order kinetic model [Eq. (33)]:

$$\frac{-dc}{dt} = k_c \cdot C \tag{33}$$

Higher nZVC concentration favors the passivation phenomena of PS and consequently, reduces the furfural decomposition rate. In these reaction orders, increasing concentration of oxidizing agent increased the reaction rate [56]. In addition, the kinetic energy of materials was increased with increasing PS, temperature and thus it can increase the reaction rate as well.

3.2.12. Artificial neural network modeling

ANNs are the straight visions of the biology of human brain. Hence, a computation neural network includes a simple unit called neuron. Each network consists of node that indicates an artificial neuron and is connected with the other neurons to form a network in which an arrow shows a link between output and input neurons. Therefore, a calculational neural network is defined by multiple layers, and nodes of each layer transfer function. We applied 3-layered feed-forward multi layer percepteron (5:7:1) for modeling AOP treatment of furfural by PS/nZVC (Fig. 1). In order to characterize the optimum number of hidden nodes, a series of topologies was tested where the number of nodes was changed [24]. Each topology was reiterated 7 times, due to the random initialization of the weights to avoid random correlation. The mean square error (MSE) was applied as an error function.

$$MSE = \frac{\sum_{i=1}^{i=N} (Y_{i,pred} - Y_{i,\exp})^2}{N} \tag{34}$$

where N is the number of data point, $Y_{i,pred}$ is the network prediction, $Y_{i,\exp}$ is the experimental response and i is an index of data. A trial and error system was done to find the suitable number of neurons in a hidden layer, in terms of MSE reduction. According to Fig. 10, the mean square belongs to 5 neurons. In this study, the tan-sigmoid and linear transfer function were applied for transfer function in hidden and output layers. Tan-sigmoid is defined by Eq. (35) as follows:

$$F(x) = \frac{1}{1 + \exp^{(-x)}} \tag{35}$$

where, $f(x)$ is the hidden neuron output. The range of effective factors determined in previous section is listed in Fig.1 [24]. The data used in this study were divided into three sets including 180 samples for training, 56 samples for validation and 56 samples for test [23]. The validation and test sets as a scale of the validation and modelling power of the network were chosen from the experimental data. All samples were normalized in the range of 0–1. Therefore, all normalized data sets (Z_i) (from the training, validation and test sets) were graduated to a novel value X_i by Eq. (36) [24].

$$Z_i = \frac{X_i - X_{\min}}{X_{\max} - X_{\min}} \tag{36}$$

In order to predict modeling errors, all outputs were accomplished in a reverse range scaling to return the forecast responses to their original scale and compare them with experimental responses (Fig. 10a) [23]. Fig. 10b indicates a comparison between the predicted and experimental values of the output variables with neural network model. We applied two lines to indicate the accuracy of prediction. One of them is the complete fit on which all the data of a desired model should lie. Another one is the excellent fits the data of the scatter plot via equation $y = ax + b$ and it is acquired via regression analysis, according to the minimization of the squared errors [23,24]. Coefficient of determination (R^2) is 0.98. The weight matrix of trained neural network was applied to find the relative importance of the various input variables on the output variables using the following equation:

$$I_j = \frac{\sum_{m=1}^{m=N_h} \left(\left(\left| W_{jm}^{ih} \right| / \sum_{k=1}^{N_i} \left| W_{km}^{ih} \right| \right) \times \left| W_{mn}^{ho} \right| \right)}{\sum_{k=1}^{k=N_i} \left\{ \sum_{m=1}^{m=N_h} \left(\left| W_{km}^{ih} \right| / \sum_{k=1}^{N_i} \left| W_{km}^{ih} \right| \right) \times \left| W_{mn}^{ho} \right| \right\}} \tag{37}$$

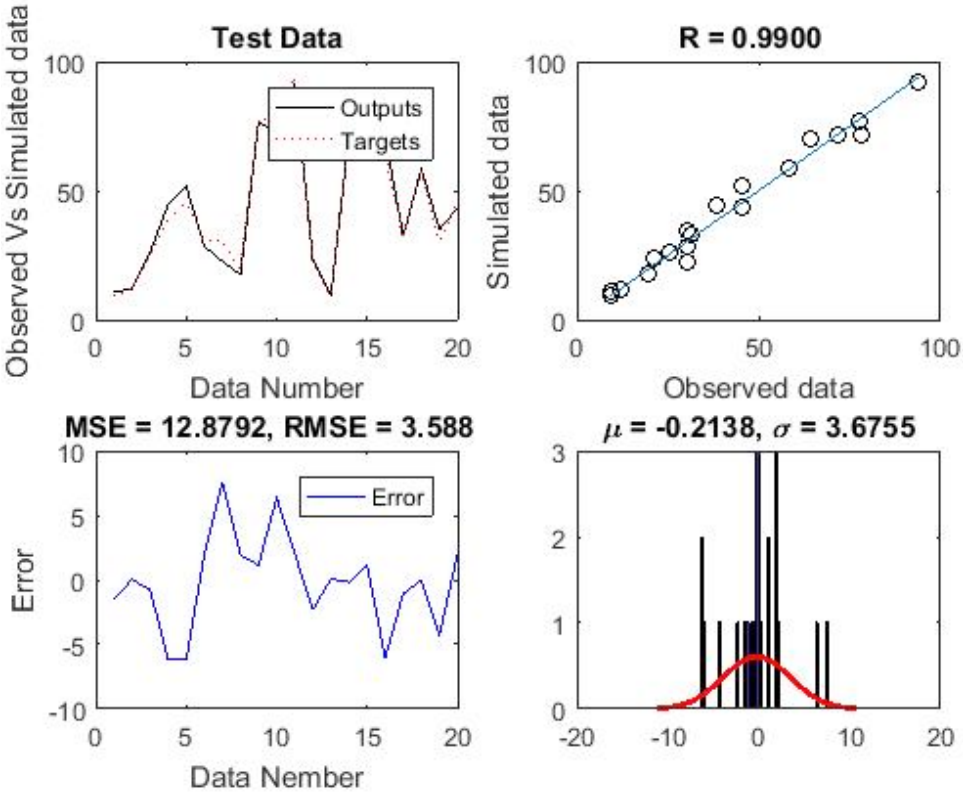

(a)

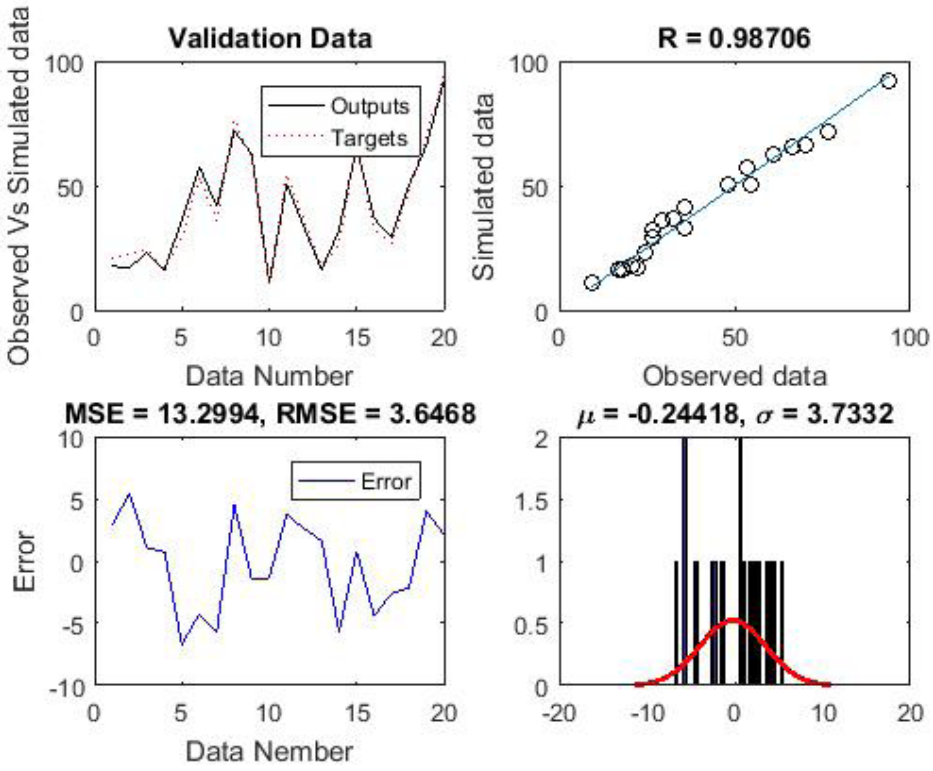

(b)

Fig. 10. Comparison between the experimental and obtained data from neural network modeling for the train sets. (b) validation sets.

Table 1
A summary of similar study from removal of furfural and PS/ZVC process

References	Pollutant	Process	Comparison of the similar studies
Zhou et al. [35]	2,4-dichlorophenol	Peroxomonosulfate using micron zero-valent copper	Optimum pH 3.1, [2,4-DCP]0 = 5 mg/L, [ZVC]0 or [nZVC]0 = 50 mg/L, [PMS]0 = 0.5 mM, [MA]0 or [TBA]0 = 20 mM, [NP]0 = 2 mM.
Zhou et al. [47]	Organic contaminants	Persulfate using zero valent copper in acidic conditions	[BA]0 = 20 mM, [PS] = 1 mM, [nZVC]0 = 40 mg L^{-1}, [Cu^{2+}] 0 = 40 mg L^{-1}, pH0 ¼ 3.0)
Hong et al. [20]	Atrazine	Montmorillonite templated subnano-sized zero-valent copper	pH = 3, atrazine = 15 μM, and $HClO_4$ (1 M)
Liu et al. [34]	Propachlor	Ferrous and copper ion activated persulfate	Propachlor (10 mg L^{-1}), PS: (5 mM), $Cu^{2\pm}$ and $Fe^{2\pm}$ (2.5 mM) at 20°C at pH 4.0
Wang et al. [36]	Dye	Zero-valent iron and copper oxide in persulfate oxidation	[OG]0 = 0.2 mM; [PS]0 = 2 mM; ZVI = 0.1 g/L; CuO = 0.1 g/L; T = 25°C; pH = 5.0 ± 0.2
Ghanbari et al. [38]	Textile wastewater	Zero valent iron activated peroxymonosulfate: Compared with zero valent copper	3000 mg/L ZVI, 4000 mg/L ZVC, H_2O_2 and PMS of 20 mM, in case of ZVI–PMS–H_2O_2: 10 mM H_2O_2 and 10 mM PMS
Liang et al. [39]	p-chloroaniline	Copper oxidate activated persulfate	[PCA]0 = 0.5 mM, [persulfate]0 = 2.5 mM, [copper oxidate]0 = 0.5 g L^{-1}, initial pH = 7.0, temperature: about 20°C.
Raut et al. [40]	Mono chloroaromatics	Zero-valent copper	Cu0 nanoparticles: (2.5 g L^{-1}) with $NaBH_4$ (1 g L^{-1}), b) Cu0: (2.5 g L^{-1}) with ac-iPrOH at room temperature for 12 h.
Ghanbari et al. [48]	Environmental organic pollutants	Peroxymonosulfate and its activation methods	Molar ratio of oxidant to metal = 1:1, molar ratio of oxidant to triclosan = 5:1, pH = 7 and time = 10 min
Fatimah et al. [30]	Acid orange 7	Ozone/ANN	Ozone concentration: 550 mg/L, AO7: 11 mg/L, pH 7.9, temperature: 41°C

where I_j is the relative importance of the j^{th} input variable on the output variable, N_i and N_h are the numbers of input and hidden neurons, respectively. W_s are connection weights, the superscript *i*, *h* and *o* refer to input, hidden and output layers, respectively, and subscript *k*, *m* and *n* refer to input, hidden and output neurons, respectively [23]. The relative importance of various variables as, computed by Eq. (37), is shown in Fig. 1. Therefore, all the input parameters have significant influence on the removal of furfural.

4. Conclusions

This work studied furfural removal from aqueous solution using nZVC particles. The degradation efficiency of furfural increased with increasing PS and nZVC concentrations. Maximum furfural removal was obtained at pH = 3 and PS = 1.2 mM. The findings of SEM revealed that the size of synthesized nanoparticles via chemical reaction approach was 25 nm. The AOP degradation efficiency was dependent on initial solution pH, reaction time, and furfural concentration. PS/nZVC degradation of furfural was performed and the intermediate compounds were recognized with FT-IR and GC-Mass techniques. In addition, results revealed that nZVC can increase the efficiency of the combination of PS with the other processes. Chemical degradation of furfural and intermediate compounds were distinguished using GC-MS technique and included ferulic acid, 2-furfural, oxime-, methoxy-phenyl, 2,2′-bifuran and cyclohexasiloxan. According to the obtained results, a three-layered neural network via 7 neurons in the hidden layer was successfully applied for prediction of furfural removal efficiency using PS/nZVC process as a novel form of AOPs.

Acknowledgments

This study was supported financially by Research Department of Ahvaz University of Medical Sciences (Grant number: 95s85).

References

[1] X. Shi, W. Ruan, J. Hu, M. Fan, R. Cao, X. Wei, Optimizing the removal of rhodamine B in aqueous solutions by reduced graphene oxide-supported nanoscale zerovalent iron (nZVI/rGO) using an artificial neural network-genetic algorithm (ANN-GA), Nanomaterials, 7 (2017) 134.
[2] M. Fan, J. Hu, R. Cao, K. Xiong, X. Wei, Modeling and prediction of copper removal from aqueous solutions by nZVI/rGO magnetic nanocomposites using ANN-GA and ANN-PSO, Sci Rep., 7 (2017) 18040.
[3] A.A. Babaei, A.R. Rahmani, F. Zamani, H. Almasi, Fe (III)–oxalate-mediated solar degradation of furfural in the presence of persulfate: operational parameters and artificial neural network modeling, J. Iran. Chem. Soc., 2 (2018) 219–229.
[4] S. Singh, V.C. Srivastava, I.D. Mall, Fixed-bed study for adsorptive removal of furfural by activated carbon, Colloids Surf. A Physicochem. Eng., 332 (2009) 50–56.

[5] A.K. Sahu, I.D. Mall, V.C. Srivastava, Studies on the adsorption of furfural from aqueous solution onto low-cost bagasse fly ash, Chem. Eng. Commun., 195 (2007) 316–335.
[6] B. Ghasemi, B. Anvaripour, S. Jorfi, N. Jaafarzadeh, Enhanced photocatalytic degradation and mineralization of furfural using UVC/TiO_2/GAC composite in aqueous solution, Int. J. Photoenergy, 2016 (2016).
[7] M. Faramarzpour, M. Vossoughi, M. Borghei, Photocatalytic degradation of furfural by titania nanoparticles in a floating-bed photoreactor, Chem. Eng. J., 146 (2009) 79–85.
[8] S. Borghei, S. Hosseini, Comparison of furfural degradation by different photooxidation methods, Chem. Eng. J., 139 (2008) 482–488.
[9] A.R. Rahmani, A. Poormohammadi, F. Zamani, Y.T. Birgani, S. Jorfi, S. Gholizadeh, M.J. Mohammadi, H. Almasi, Activated persulfate by chelating agent Fe·/complex for in situ degradation of phenol: intermediate identification and optimization study, Res. Chem. Intermed., 44 (2018) 5501–5519.
[10] R.R. Kalantary, A. Mohseni-Bandpi, A. Esrafili, S. Nasseri, F.R. Ashmagh, S. Jorfi, M. Ja'fari, Effectiveness of biostimulation through nutrient content on the bioremediation of phenanthrene contaminated soil, J. Environ. Health Sci. Eng., 12 (2014) 143.
[11] S.-H. Do, Y.-J. Kwon, S.-J. Bang, S.-H. Kong, Persulfate reactivity enhanced by Fe_2O_3–MnO and CaO–Fe_2O_3–MnO composite: identification of composite and degradation of CCl_4 at various levels of pH, Chem. Eng. J., 221 (2013) 72–80.
[12] S.-H. Do, Y.-J. Kwon, S.-J. Bang, S.-H. Kong, Persulfate reactivity enhanced by Fe_2O_3–MnO and CaO–Fe_2O_3–MnO composite: Identification of composite and degradation of CCl_4 at various levels of pH, Chem. Eng. J, 221 (2013) 72–80.
[13] M. Sadrnourmohamadi, A. Poormohammadi, H. Almasi, G. Asgari, A. Ahmadzadeh, A. Seid-Mohammadi, Removal of 2, 4-dichlorophenol from aqueous solution using ultrasonic/H, Desal. Water Treat., 75 (2017) 189–194.
[14] X. Gu, Y. Wang, Z. Miao, S. Lu, Z. Qiu, Q. Sui, X. Guo, Degradation of trichloroethylene in aqueous solution by persulfate activated with Fe(III)–EDDS complex, Res. Chem. Intermed., 43 (2017) 1–13.
[15] C. Cai, Z. Zhang, H. Zhang, Electro-assisted heterogeneous activation of persulfate by Fe/SBA-15 for the degradation of Orange II, J. Hazard. Mater., 313 (2016) 209–218.
[16] A.R. Rahmani, F. Zamani, A. Shabanloo, H. Almasi, Effect of silica on the ultrasonic/persulfate process for degradation of Acid Black 1 in aqueous solutions, Avicenna J. Environ. Health Eng., 3 (2016) 1–6.
[17] Z. Issaabadi, M. Nasrollahzadeh, S.M. Sajadi, Green synthesis of the copper nanoparticles supported on bentonite and investigation of its catalytic activity, J. Cleaner Prod., 142 (2017) 3584–3591.
[18] X. Du, Y. Zhang, I. Hussain, S. Huang, W. Huang, Insight into reactive oxygen species in persulfate activation with copper oxide: activated persulfate and trace radicals, Chem. Eng. J., 313 (2017) 1023–1032.
[19] P. Zhou, J. Zhang, J. Liu, Y. Zhang, J. Liang, Y. Liu, B. Liu, W. Zhang, Degradation of organic contaminants by activated persulfate using zero valent copper in acidic aqueous conditions, RSC Adv., 6 (2016) 99532–99539.
[20] R. Hong, Z. Guo, J. Gao, C. Gu, Rapid degradation of atrazine by hydroxyl radical induced from montmorillonite templated subnano-sized zero-valent copper, Chemosphere, 180 (2017) 335–342.
[21] W. Ruan, X. Shi, J. Hu, Y. Hou, M. Fan, R. Cao, X. Wei, Modeling of Malachite Green Removal from aqueous solutions by nanoscale zerovalent zinc using artificial neural network, Appl. Sci., 8 (2017) 3.
[22] A. Qishlaqi, S. Kordian, A. Parsaie, Field measurements and neural network modeling of water quality parameters, Appl. Water Sci., (2017) 1–8.
[23] A. Aleboyeh, M. Kasiri, M. Olya, H. Aleboyeh, Prediction of azo dye decolorization by UV/H_2O_2 using artificial neural networks, Dyes Pigments, 77 (2008) 288–294.
[24] A. Khataee, G. Dehghan, A. Ebadi, M. Zarei, M. Pourhassan, Biological treatment of a dye solution by Macroalgae Chara sp.: Effect of operational parameters, intermediates identification and artificial neural network modeling, Bioresour. Technol., 101 (2010) 2252–2258.
[25] A.R. Esfahani, S. Hojati, A. Azimi, M. Farzadian, A. Khataee, Enhanced hexavalent chromium removal from aqueous solution using a sepiolite-stabilized zero-valent iron nanocomposite: impact of operational parameters and artificial neural network modeling, J. Taiwan Inst. Chem. Eng., 49 (2015) 172–182.
[26] A. Ghaedi, Simultaneous prediction of the thermodynamic properties of aqueous solution of ethylene glycol monoethyl ether using artificial neural network, J. Mol. Liq., 207 (2015) 327–333.
[27] A.M. Ghaedi, A. Vafaei, Applications of artificial neural networks for adsorption removal of dyes from aqueous solution: a review, Adv. Colloid Interface Sci., 245 (2017) 20–39.
[28] R. Mittu, Synthesis, Characterization of copper nanoparticles-a review, Synthesis, 3 (2016) 37–40.
[29] P. Rahimi, H. Hashemipour, M. Ehtesham Zadeh, S. Ghader, Experimental investigation on the synthesis and size control of copper nanoparticle via chemical reduction method, Int. Nanosci. Nanotechnol., 6 (2010) 144–149.
[30] S. Fatimah, W. Wiharto, The use of artificial neural network for modeling the decolourization of acid orange 7 solution of industrial by ozonation process, in: IOP Conference Series: Materials Science and Engineering, IOP Publishing, 2017, pp. 012052.
[31] M. Raja, J. Subha, F.B. Ali, S.H. Ryu, Synthesis of copper nanoparticles by electroreduction process, Mater. Manuf. Process., 23 (2008) 782–785.
[32] Y. Suresh, S. Annapurna, G. Bhikshamaiah, A. Singh, Copper nanoparticles: green synthesis and characterization, Int. J. Sci. Eng. Res., 5 (2014) 156–160.
[33] Z.N. Kayani, M. Umer, S. Riaz, S. Naseem, Characterization of copper oxide nanoparticles fabricated by the sol-gel method, J. Electron. Mater., 44 (2015) 3704–3709.
[34] C. Liu, K. Shih, C. Sun, F. Wang, Oxidative degradation of propachlor by ferrous and copper ion activated persulfate, Sci. Total. Environ., 416 (2012) 507–512.
[35] P. Zhou, J. Zhang, Y. Zhang, G. Zhang, W. Li, C. Wei, J. Liang, Y. Liu, S. Shu, Degradation of 2, 4-dichlorophenol by activating persulfate and peroxomonosulfate using micron or nanoscale zero-valent copper, J. Hazard. Mater., 344 (2018) 1209–1219.
[36] C. Wang, J. Wan, Y. Ma, Y. Wang, Insights into the synergy of zero-valent iron and copper oxide in persulfate oxidation of Orange G solutions, Res. Chem. Intermed., 42 (2016) 481–497.
[37] H. Li, J. Wan, Y. Ma, Y. Wang, Reaction pathway and oxidation mechanisms of dibutyl phthalate by persulfate activated with zero-valent iron, Sci. Total Environ., 562 (2016) 889–897.
[38] F. Ghanbari, M. Moradi, M. Manshouri, Textile wastewater decolorization by zero valent iron activated peroxymonosulfate: compared with zero valent copper, J. Environ. Chem. Eng., 2 (2014) 1846–1851.
[39] H.-y. Liang, Y.-q. Zhang, S.-b. Huang, I. Hussain, Oxidative degradation of p-chloroaniline by copper oxidate activated persulfate, Chem. Eng. J., 218 (2013) 384–391.
[40] S.S. Raut, S.P. Kamble, P.S. Kulkarni, Efficacy of zero-valent copper (Cu0) nanoparticles and reducing agents for dechlorination of mono chloroaromatics, Chemosphere, 159 (2016) 359–366.
[41] A.R. Rahmani, F. Zamani, Z. Masoumi, R. Harati, H. Almasi, Investigation of phenol removal of phenol by electro/fenton and electro/persulfate in aqueous solution, Water Wastewater, 5 (2016) 38–45.
[42] A. Alba-Rubio, J. Fierro, L. León-Reina, R. Mariscal, J. Dumesic, M.L. Granados, Oxidation of furfural in aqueous H_2O_2 catalysed by titanium silicalite: Deactivation processes and role of extra framework Ti oxides, Appl. Catal. B: Environ., 202 (2017) 269–280.
[43] H. Gao, J. Chen, Y. Zhang, X. Zhou, Sulfate radicals induced degradation of Triclosan in thermally activated persulfate system, Chem. Eng. J., 306 (2016) 522–530.

[44] Y. Wu, R. Prulho, M. Brigante, W. Dong, K. Hanna, G. Mailhot, Activation of persulfate by Fe (III) species: Implications for 4-tert-butylphenol degradation, J. Hazard. Mater., 322 (2017) 380–386.
[45] A. Rezaee, H. Godini, S. Jorfi, Nitrate removal from aqueous solution using $MgCl_2$ impregnated activated carbon, Environ. Eng. Manag. J., 9 (2010) 449–452.
[46] Z. Wang, R. Yuan, Y. Guo, L. Xu, J. Liu, Effects of chloride ions on bleaching of azo dyes by Co^{2+}/oxone regent: kinetic analysis, J. Hazard. Mater., 190 (2011) 1083–1087.
[47] P. Zhou, B. Liu, J. Zhang, Y. Zhang, G. Zhang, C. Wei, J. Liang, Y. Liu, W. Zhang, Radicals induced from peroxomonosulfate by nanoscale zero-valent copper in the acidic solution, Water Sci. Technol., 74 (2016) 1946–1952.
[48] F. Ghanbari, M. Moradi, Application of peroxymonosulfate and its activation methods for degradation of environmental organic pollutants: Review, Chem. Eng. J., 310 (2017) 41–62.
[49] H. Almasi, G. Asgari, M. Leili, Z. Sharifi, A. Seid-Mohammadi, The study of phenol removal from aqueous solutions using oxidizing agents of peroxide hydrogen, persulfate and periodate activated by ultrasound, J. Rafsanjan Univ. Med. Sci., 15 (2017) 835–848.
[50] D. ASTM, 1252-. 06, Chemical Oxygen Demand (Dichromate Oxygen Demand) of Water, Test Method B.
[51] C.-l. Kang, X.-j. Tang, X.-q. Jiao, P. Guo, F.-m. Quan, X.-y. Lin, Degradation of furfural by UV/O_3 technology, Chem. Res. Chinese U, 25 (2009) 451–454.
[52] D. Mantzavinos, E. Lauer, M. Sahibzada, A.G. Livingston, I.S. Metcalfe, Assessment of partial treatment of polyethylene glycol wastewaters by wet air oxidation, Water Res., 34 (2000) 1620–1628.
[53] R.D.C. Soltani, S. Jorfi, H. Ramezani, S. Purfadakari, Ultrasonically induced ZnO–biosilica nanocomposite for degradation of a textile dye in aqueous phase, Ultrason. Sonochem., 28 (2016) 69–78.
[54] W.H. Organization, Copper in drinking water. Background document for preparation of WHO guidelines for drinking-water quality, WHO: Geneva, Switzerland, 2003.
[55] D. Raharinirina, G. Ramanantsizehena, F.L. Razafindramisa, N.K.V. Leitner, Comparison of UV/H_2O_2 and UV/S_2O_8 2-processes for the decoloration of azo dyes Congo Red in various kinds of water, in: Fourth High-Energy Phys. Int. Conf., 2009.
[56] J.E. Silveira, T.O. Cardoso, M. Barreto-Rodrigues, J.A. Zazo, J.A. Casas, Electro activation of persulfate using iron sheet as low-cost electrode: the role of the operating conditions, Environ. Technol., 9 (2018) 1208–1216.